

## ABILITY OF LOCALIZING GRADIENT DAMAGE TO DETERMINE SIZE EFFECT IN CONCRETE BEAMS<sup>1</sup>

ADAM WOSATKO, JERZY PAMIN, ANDRZEJ WINNICKI

*Cracow University of Technology, Faculty of Civil Engineering, Cracow, Poland*

*e-mail: adam.wosatko@pk.edu.pl; jerzy.pamin@pk.edu.pl; andrzej.winnicki@pk.edu.pl*

The objective of the paper is to demonstrate the potential of the localizing gradient damage model in size effect simulations. Three different gradient activity functions for variable internal length scale are considered. Numerical simulations for an unnotched beam under three-point bending are referred to the experiment performed by Grégoire *et al.* (2013). A confrontation with the conventional gradient damage model as well as mesh sensitivity studies are also presented. It is proved that the localizing gradient damage model with different variants of the gradient activity function can reproduce the size effect quite reasonably.

*Keywords:* size effect, concrete, localizing gradient damage, finite element method

### 1. Introduction

The size effect is connected with a change of the material response, which is observed for structural elements or laboratory specimens with different volumes. In quasi-brittle materials like concrete, it is observed that the nominal strength decreases when the size of the considered specimen enlarges. An analogical relation is also observed for equilibrium paths in the post-peak regime, taking into account material brittleness. In fact, the size of the fracture process zone (FPZ) in quasi-brittle materials like concrete does not correspond to the dimensions of structural elements, instead it is related to the material length scale. The main cause of the size effect is deterministic and related to the rate of energy dissipation in FPZ and evolving cracks, see e.g. (Bažant and Planas, 1998).

The above statements are proven in many experiments, hence the deterministic size effect is one of crucial features examined for quasi-brittle materials. Together with the development of fracture and damage theories, the knowledge about the size effect laws has also been improved, see e.g. (Bažant and Le, 2017; Bažant and Planas, 1998). When the size effect is analyzed numerically, standard local models are not able to capture it properly. Therefore, correct computational models for concrete should be equipped with a localization limiter, i.e. contain an internal length scale. There are several approaches to ensure mesh-objective results for continuum models. The first option, followed in this paper, is to use a non-local formulation via integral or gradient-type averaging. The second concept is to introduce a rate-dependence into the constitutive relation. The simplest approach is the crack band theory, proposed first by Bažant and Oh (1983), which however is not a proper localization limiter since it alleviates only the mesh sensitivity of load-displacement diagrams. A complementary overview of these issues can be found, for instance, in (Bažant and Jirásek, 2002).

In this paper, the damage model is enhanced by the presence of higher-order gradients via an averaging equation in the formulation based on continuum damage mechanics. The gradient

---

<sup>1</sup>Paper presented during PCM-CMM 2023

damage model was first suggested by Peerlings *et al.* (1996). In the description of finite elements (FEs), two types of degrees of freedom are distinguished, i.e. an averaged strain measure is approximated next to the standard displacement field. The zone of localization represents concrete cracking in the model and it is controlled by a constant internal length scale. The interpretation of the internal length scale as constant in quasi-brittle materials can be connected with the maximum aggregate size as a counterpart of the width of the FPZ, see e.g. (Bažant and Planas, 1998). The conventional gradient damage (CGD) model ensures mesh-objective results, but Geers (1997) demonstrated that artificially expanding damage zones could occur, hence versions of the gradient damage model with evolving internal length scale have been proposed as more correct. In other words, the issue of spuriously widened damage zones is mitigated when the internal length scale becomes a variable. In this case, the model needs a definition of the so-called gradient activity function. The early concept is that the gradient activity increases as a function of an equivalent strain, see e.g. (Geers, 1997; Saroukhani *et al.*, 2013). However, if a localization phenomenon is observed during the loading process, then the interaction region of diffuse microcracks diminishes and tends to the formation of one macrocrack. From this point of view, the localizing gradient damage (LGD) model, proposed first by Poh and Sun (2017), where the gradient activity function decreases with damage growth, describes the change of the internal length scale in a more proper way. Nowadays, the LGD model is employed in many applications, e.g. it can be coupled with three-surface cap plasticity, as derived by Zhao *et al.* (2023) or used for simulations with impact loading, see (Wosatko, 2022).

In this paper, attention is focused on simulations of the size effect for beams subjected to three-point bending. Grégoire *et al.* (2013) performed experiments for unnotched (Type 1) and notched (Type 2) concrete beams using four sizes of specimens, and next analyzed them numerically by means of a non-local integral-type damage model. Other experimental tests of concrete beams under three-point bending were studied by Hoover *et al.* (2013), where four different sizes and five different options of notch depth were considered. Experiments for eccentrically notched beams (the notch is not located directly under the load) together with corresponding simulations using the discrete crack model with interface FEs were discussed by García-Álvarez *et al.* (2012). The aforementioned experimental research on the size effect was comprehensively verified in computations. A phase-field damage model equipped with additional approximation to regularize a crack surface was investigated by Feng and Wu (2018). An isotropic damage model with the crack width determined by the so-called Irwin's characteristic length was demonstrated by Barbat *et al.* (2020). In the model, a mixed FE formulation with the interpolation of displacement and strain fields as well as a stabilization strategy were employed. The size effect has also been explored using different versions of gradient damage models. For example, the size effect can help one to estimate characteristic parameters of the CGD model as shown by Carmeliet (1999). Size effect simulations given by Zhang *et al.* (2021) in confrontation with the experiments (Grégoire *et al.*, 2013; Hoover *et al.*, 2013) presented the applicability of the LGD model. The analysis of the energy dissipation during the loading process for the CGD and LGD models was highlighted there. The size effect can also be predicted using the stress-based LGD model (Negi *et al.*, 2021).

In this paper, the numerical analysis is limited to unnotched beams under three point bending, i.e. size effect Type 1 is simulated. The results are referred to the experiment (Grégoire *et al.*, 2013), where four different sizes of specimens were taken into account. The LGD model with different functions of gradient activity is considered and additionally compared with the CGD model. Both models are implemented by the authors in the FEAP package (Taylor, 2001). Section 2 describes briefly both versions of the gradient damage model, but definitions of the gradient activity function (including a new polynomial one) are characterized in detail. Section 3 shows the numerical analysis of the unnotched beam, where the simulation data, mesh sensitivity and size effect studies are respectively presented. The results for the LGD model with three

different gradient activity functions are discussed in the context of its ability to determine the size effect properly. A comparison with the results for the CGD model is also made. Conclusions are summarized in Section 4.

## 2. Overview of applied gradient damage models

### 2.1. Essentials of conventional gradient damage (CGD)

The standard boundary value problem (BVP) for statics is considered, where the equilibrium equation with corresponding boundary conditions is taken into account. Small strains are assumed. The model employed in this paper is based on the continuum damage mechanics theory, where in the nonlocal formulation an averaging equation with gradient terms is added to guarantee a mesh-independent solution, see (Peerlings *et al.*, 1996). The thermodynamic framework leads to weak forms of both the mentioned equations, and finally to a matrix system. More details of different variants of the gradient damage model can be found in many works, e.g. (Geers, 1997; Peerlings *et al.*, 2004; Poh and Sun 2017; Negi *et al.*, 2021; Wosatko, 2022). Below only the most crucial elements of the theory are recalled. Voigt's notation (called also matrix-vector notation) is used.

The real and effective (fictitious) configurations of a damaging body are distinguished. The concept of strain equivalence is adopted, i.e. the actual and effective strain tensors are equivalent  $\boldsymbol{\epsilon} = \hat{\boldsymbol{\epsilon}}$ . The effective stress tensor  $\hat{\boldsymbol{\sigma}}$  (introduced in a vector form) affects the undamaged material skeleton, so the stress tensor  $\boldsymbol{\sigma}$  corresponding to the real material is reduced by the presence of damage  $\omega$

$$\boldsymbol{\sigma} = (1 - \omega)\hat{\boldsymbol{\sigma}} \quad \hat{\boldsymbol{\sigma}} = \mathbf{D}\boldsymbol{\epsilon} \quad (2.1)$$

where  $\mathbf{D}$  is Hooke's operator. In the model,  $\omega$  is a scalar measure which changes from 0 for the undamaged material to 1 for its complete failure. This elastic stiffness degradation is a proper description for quasi-brittle materials like concrete. The damage activation function  $F^d$  is defined in the strain space

$$F^d(\boldsymbol{\epsilon}, \kappa^d) = \tilde{\epsilon}(\boldsymbol{\epsilon}) - \kappa^d \quad (2.2)$$

where  $\kappa^d$  is a damage history parameter and  $\tilde{\epsilon}$  is an equivalent strain measure. The function  $\tilde{\epsilon}(\boldsymbol{\epsilon})$  describes the loading process and can be defined according to the modified von Mises formula (de Vree *et al.*, 1995)

$$\tilde{\epsilon}(\boldsymbol{\epsilon}) = \frac{(k-1)I_1^\epsilon}{2k(1-2\nu)} + \frac{1}{2k} \sqrt{\left(\frac{k-1}{1-2\nu}I_1^\epsilon\right)^2 + \frac{12kJ_2^\epsilon}{(1+\nu)^2}} \quad (2.3)$$

where  $I_1^\epsilon$  and  $J_2^\epsilon$  are strain invariants,  $\nu$  is Poisson's ratio and  $k = f_c/f_t$  is the ratio of uniaxial compressive and tensile strengths, which enables different responses of the concrete model in tensile and compressive regimes, even though the scalar description is employed. Damage  $\omega$  is a function of the history parameter  $\kappa^d$  and can be defined as (Mazars and Pijaudier-Cabot, 1989)

$$\omega(\kappa^d) = 1 - \frac{\kappa_o}{\kappa^d} \left(1 - \alpha + \alpha e^{-\eta(\kappa^d - \kappa_o)}\right) \quad (2.4)$$

where  $\kappa_o$  is the damage threshold. This formula holds when  $\kappa^d > \kappa_o$ , and then damage  $\omega$  asymptotically grows to 1 according to the exponential function, which has been observed in the experiments by Hordijk (1991). The parameter  $\alpha$  sets the level of the residual stress  $(1 - \alpha)E\kappa_o$ , where  $E$  is Young's modulus. In this way, the total loss of material stiffness can be excluded.

The parameter  $\eta$  defines material brittleness in the post-peak stage and is related to concrete fracture energy  $G_f$ .

In the conventional gradient damage (CGD) model, the damage activation function defined in Eq. (2.2) takes the following form

$$F^d(\boldsymbol{\epsilon}, \kappa^d) = \bar{\epsilon}(\tilde{\epsilon}(\boldsymbol{\epsilon})) - \kappa^d \quad (2.5)$$

and the averaged (nonlocal) strain  $\bar{\epsilon}$  is a function of the equivalent strain  $\tilde{\epsilon}$  via the following differential equation (Peerlings *et al.*, 1996)

$$\bar{\epsilon} - \varphi \nabla^2 \bar{\epsilon} = \tilde{\epsilon} \quad (2.6)$$

The BVP problem becomes regularized by the presence of  $\bar{\epsilon}$  together with its second gradient in this averaging equation. For a domain  $\mathcal{B}$ , the natural boundary condition  $\mathcal{N}^T \nabla \bar{\epsilon} = 0$  holds on the boundary  $\partial \mathcal{B}$  ( $\mathcal{N}$  is the outward normal to the surface of domain  $\mathcal{B}$ ). It is assumed that the gradient is scaled by  $\varphi > 0$ . This quantity is constant in the CGD model and denoted in this paper by the parameter  $\varphi_s$ , which is equivalent to  $c$  and related to the square of internal length scale  $l$

$$\varphi_s = c = \frac{1}{2} l^2 \quad (2.7)$$

The internal length scale sets the localization band width (Geers, 1997; Peerlings *et al.*, 1996).

## 2.2. Localizing gradient damage (LGD) and gradient activity functions

In the localizing gradient damage (LGD) model, originally given by Poh and Sun (2017), the quantity  $\varphi$  becomes a variable and is called the gradient activity function. The averaging equation is rewritten as follows

$$\bar{\epsilon} - \nabla(\varphi \nabla \bar{\epsilon}) = \tilde{\epsilon} \quad (2.8)$$

The above equation can be derived from a microforce balance, but here additional effects of micro-macro scale interaction, connected with the definition of a coupling stress, are not considered. The thermodynamic framework of the LGD model can be found e.g. in (Negi *et al.*, 2021; Poh and Sun, 2017; Wosatko, 2022). More detailed derivations and different aspects of implementation of this model are discussed, for example, by Wang *et al.* (2002) and Wosatko (2022). After discretization of the weak form and linearization of the BVP, it turns out that an additional matrix operator has to be computed in the matrix system of equations, where the derivative of  $\varphi$  is needed. Some proposals of gradient activity functions together with their derivatives are listed below.

When the LGD model is employed, the gradient activity is a function of damage  $\omega$ . It is illustrated by Poh and Sun (2017), Wosatko (2022) that the influence of nonlocal interactions in the localization region should decrease with the increase of damage. It is observed that the crack band width gradually reduces and the model tends to the local one, so its localizing character reveals. The first formula for the gradient activity function is defined by Poh and Sun (2017) and includes exponential terms

$$\varphi_e(\omega) = c_{max} \frac{(1 - R) \exp(-n\omega) + R - \exp(-n)}{1 - \exp(-n)} \quad (2.9)$$

In Eq. (2.9),  $c_{max}$  is the maximum internal length scale squared,  $R$  is the (minimum) residual level of nonlocal interaction and  $n$  is the power which changes the rate of decrease of the inter-

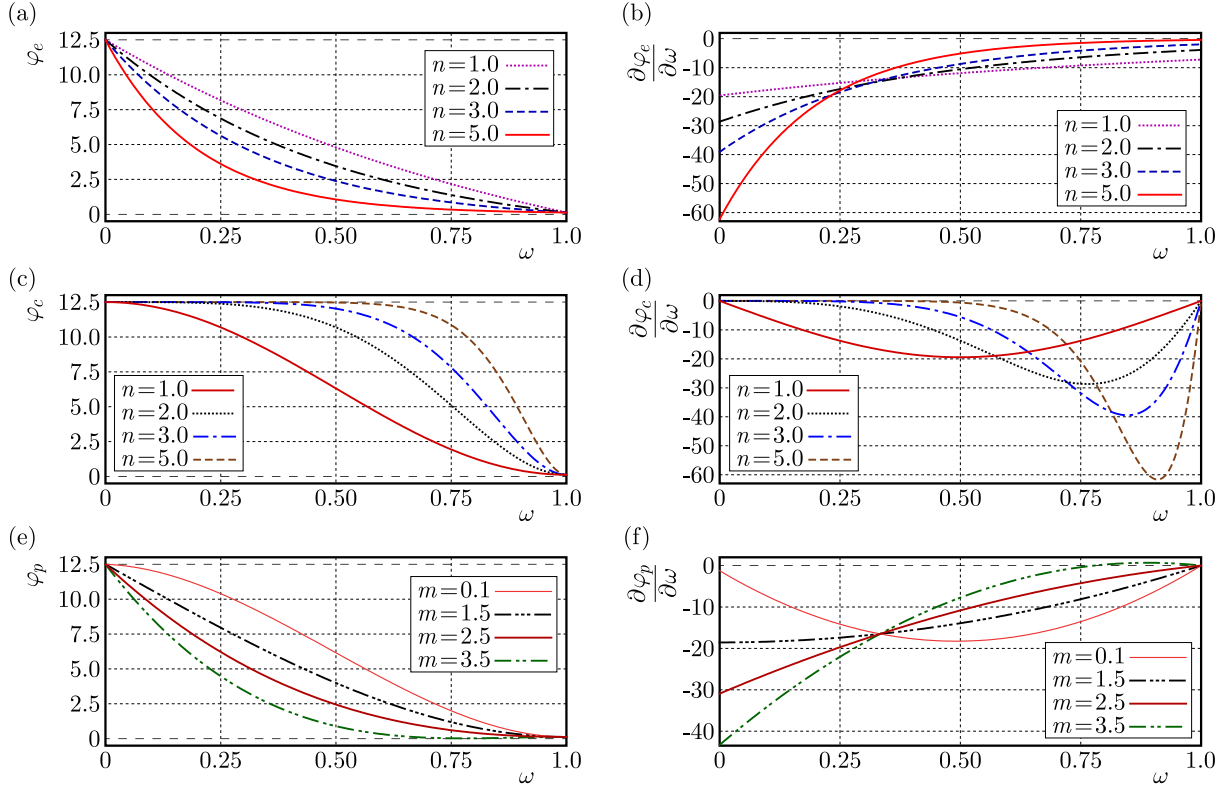


Fig. 1. Gradient activity functions and their derivatives for different values of  $n$  or  $m$ : (a) function  $\varphi_e$ , (b) derivative  $\partial\varphi_e/\partial\omega$ , (c) function  $\varphi_c$ , (d) derivative  $\partial\varphi_c/\partial\omega$ , (e) function  $\varphi_p$ , (f) derivative  $\partial\varphi_p/\partial\omega$

action, which can be shortly called the intensity parameter. This function is depicted in Fig. 1a in diagrams with different  $n$  ( $c_{max} = 12.5 \text{ mm}^2$  and  $R = 0.01$ ). The derivative of function  $\varphi_e$  is

$$\frac{\partial\varphi_e}{\partial\omega} = c_{max} \frac{(R-1)n \exp(-n\omega)}{1 - \exp(-n)} \quad (2.10)$$

Figure 1b presents diagrams of this derivative for analogical cases. There are possible alternative definitions of the gradient activity function. The relation  $\varphi(\omega)$  and its derivative can be defined by means of cosine and sine functions as proposed by Wosatko (2022)

$$\begin{aligned} \varphi_c(\omega) &= c_{max} \left[ \frac{1}{2} (\cos(\pi\omega^n) + 1)(1-R) + R \right] \\ \frac{\partial\varphi_c}{\partial\omega} &= \frac{1}{2} \pi c_{max} n (R-1) \omega^{(n-1)} \sin(\pi\omega^n) \end{aligned} \quad (2.11)$$

Figures 1c and 1d illustrate both the definitions for  $c_{max} = 12.5 \text{ mm}^2$  and  $R = 0.01$ . It should be noticed that if  $n > 1.0$  then the start of the decreasing interaction process is postponed. For example, for intensity  $n = 5.0$ , the value of  $\varphi_c$  is effectively reduced only after  $\omega > 0.5$ . The intentional retardation of this reduction is introduced by Wang *et al.* (2022) using function  $\varphi_e(\omega)$  from Eq. (2.9), governed by an additional threshold for damage, so that the cracking in fiber reinforced ultra-high performance concrete beams can be simulated. The change of the interaction area within the localization region should be delayed for special concrete materials. As shown in Fig. 1d, for each  $n$ , the derivative  $\partial\varphi_c/\partial\omega$  starts from the value 0.0 for  $\omega = 0.0$  as well as it is equal to 0.0 for  $\omega = 1.0$  at the end. It seems that the derivative should be zeroed especially in the final stage of failure ( $\omega = 1.0$ ), when further damage increment is not possible. Another formula comes from the phase-field approach (Borden, 2012; de Borst and

Verhoosel, 2016), where the gradient activity function with polynomial terms is written based on the so-called degradation function

$$\varphi_p(\omega) = c_{max}\{[(m-2)(1-\omega)^3 + (3-m)(1-\omega)^2](1-R) + R\} \quad (2.12)$$

where  $m$  is a weighting factor of the polynomials. The derivative of function  $\varphi_p$  is

$$\frac{\partial \varphi_p}{\partial \omega} = c_{max}(1-R)[(6-3m)\omega^2 + (4m-6)\omega - m] \quad (2.13)$$

Figure 1e presents the function from Eq. (2.12) in diagrams for  $c_{max} = 12.5 \text{ mm}^2$ ,  $R = 0.01$  and with different factors  $m$ , while in Fig. 1f the corresponding derivatives defined in Eq. (2.13) are drawn. When the value of  $m$  is 0.1 or smaller (not presented here), then the function  $\varphi_p$  is similar to  $\varphi_c$  with  $n = 1.0$ . In fact, it resembles a cosine function. On the other hand, when  $m = 1.5$  or larger, then the function  $\varphi_p$  is similar to the function  $\varphi_e$  given in Eq. (2.9). From this point of view, it seems that the function  $\varphi_p$  has the most universal form. It should be noted that red curves in Fig. 1 represent cases employed in the computations in the next Section.

### 3. Numerical study of unnotched beam under three point bending

#### 3.1. Geometry and material model data

The numerical example discussed in this Section is based on the experiment conducted by Grégoire *et al.* (2013). The left symmetric half of the domain is taken into account. Figure 2 depicts configuration of the beam subjected to three point bending. Mesh M3, which is applied in the size effect study with identical density for each specimen, is also illustrated in Fig. 2. The dimensions of four specimens are summarized in Table 1. The thickness  $T = 50 \text{ mm}$  is the same for all considered cases. The following mesh densities are used: mesh M1 includes 1260 nodes and 1065 FEs, M2 – 4610 nodes and 4230 FEs, M3 – 17615 nodes and 16860 FEs, M4 – 65153 nodes and 63740 FEs. Mesh M4 is prepared only for the LGD model. Four-noded FEs with linear interpolation of the displacement field and the averaged strain measure are adopted.

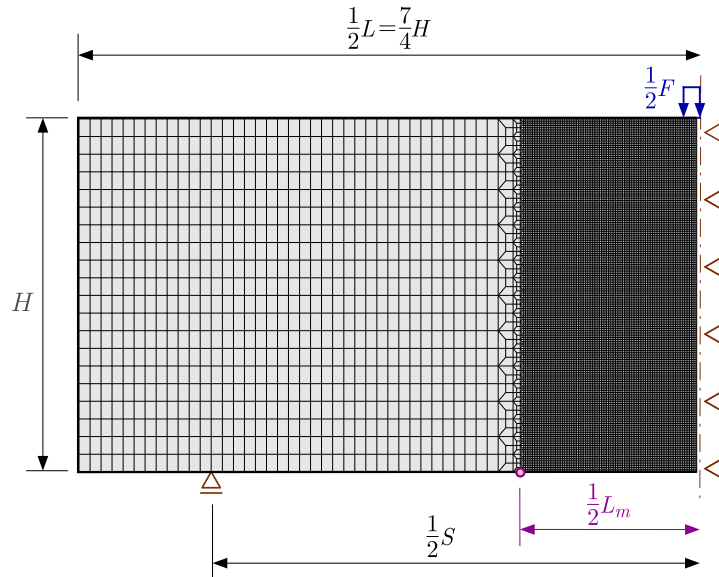


Fig. 2. Configuration of the symmetric half of the unnotched beam in three point bending and mesh M3

Plane stress conditions hold. Young's modulus  $E = 37000 \text{ MPa}$  and Poisson's ratio  $\nu = 0.21$  are assumed for concrete. The threshold  $\kappa_o = 0.0000946$  for the damage growth function in

**Table 1.** Geometry of specimens

Specimen	Length $L$ [mm]	Height $H$ [mm]	Span $S$ [mm]	Measurement base $L_m$ [mm]
D1	1400	400	1000	400
D2	700	200	500	200
D3	350	100	250	100
D4	175	50	125	50

Eq. (2.4) corresponds to the tensile strength  $f_t = 3.5$  MPa. The modified von Mises definition given in Eq. (2.3) is determined with the ratio  $k = 12.086$ , which means that the compressive strength is indirectly defined as  $f_c = 42.3$  MPa. The parameter  $\alpha = 0.99$  is adopted for all computations. It is known that the same value of parameter  $\eta$  provides different behaviour for CGD and LGD models. The results for the LGD model give a much more brittle response, see e.g. (Poh and Sun, 2017), so the value of  $\eta$  connected with the rate of damage growth should be several times smaller than for the CGD model. Respectively, values 300 and 85 are applied. All the cases considered in the computations are listed in Table 2. Acronyms are connected with the CGD or LGD models and the choice of the gradient activity function  $\varphi$ . The parameters  $R$  and  $n$  or  $m$  are suitable for the given function. The internal length scale squared  $c_{max} = 12.5$  mm<sup>2</sup> is used in each case, but as a constant in the CGD model or as the maximum in the LGD model. For the CGD model, it simply means that  $l = 5$  mm. The options mentioned in Table 2 for the LGD model coincide with the red curves depicted in Fig. 1.

**Table 2.** Computational cases for size effect analysis

Case	Model				
	$\eta$	Function $\varphi$	Gradient activity	$R$	$n$ or $m$
CGD	300	$\varphi_s$	constant	–	–
LGD-e	85	$\varphi_e(\omega)$	exponential	0.01	5.0
LGD-c	85	$\varphi_c(\omega)$	cosine	0.01	1.0
LGD-p-01	85	$\varphi_p(\omega)$	polynomial	0.01	0.1
LGD-p-25	85	$\varphi_p(\omega)$	polynomial	0.01	2.5

### 3.2. Mesh sensitivity study

Firstly, the numerical analysis is focused on the demonstration of the mesh-objective solution for both versions of the gradient damage model. Only specimen D3 is considered in this study. Figure 3 presents the diagrams of force  $F$  applied to the beam versus horizontal displacement  $u_{hor}$ , called also a pseudo-CMOD (crack mouth opening displacement), measured at the bottom edge between two points specified over the base  $L_m$ . A half of this base together with one point marked by a purple circle is illustrated in Fig. 2.

It is visible in Fig. 3a that all curves for the CGD model overlap, but simultaneously they deviate from the experiment. The contour plots for damage  $\omega$  at the final stage are depicted in Fig. 4. It is seen that the same representation is obtained for each mesh. The most damaged region, where  $\omega \rightarrow 1.0$ , is illustrated by the black colour. All distributions of damage for the CGD model are quite spread. Therefore, the problem of too strongly broadened damage zone in the CGD model is confirmed, see also (Geers, 1997; Poh and Sun, 2017; Wosatko, 2022; Zhang *et al.*, 2021).

Figure 3b shows the equilibrium paths only for case LGD-p-25 with  $\varphi_p(\omega)$  and  $m = 2.5$ . The mesh sensitivity study for the LGD model with functions  $\varphi_e$  and  $\varphi_c$  can be found in (Wosatko,

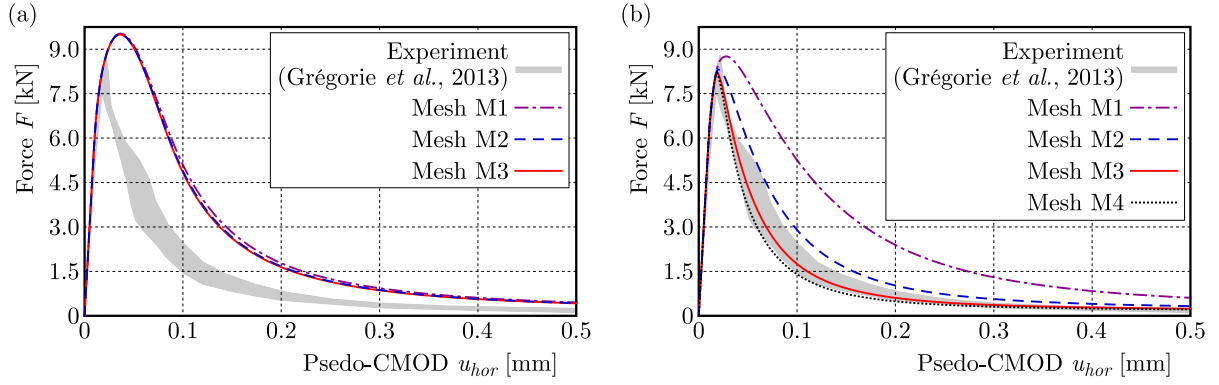


Fig. 3. Load vs. pseudo-CMOD diagrams, mesh-sensitivity study: (a) CGD, (b) LGD-p-25

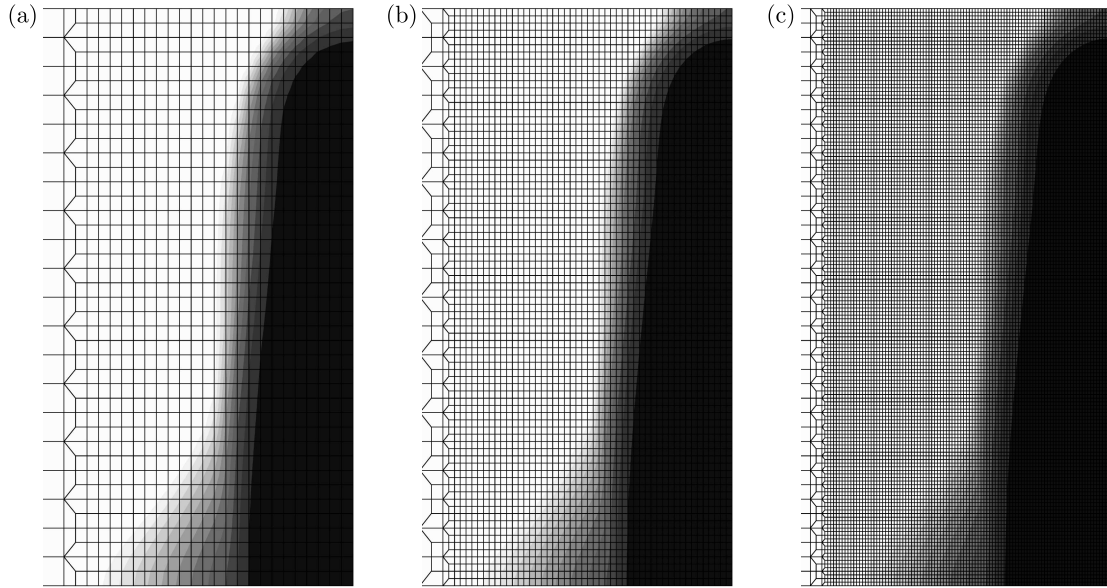


Fig. 4. Contour plots of damage  $\omega$  for CGD, mesh-sensitivity study: (a) mesh M1, (b) mesh M2, (c) mesh M3

2022). It can be noticed here that the diagrams differ from each other, but the responses for M3 and M4 almost coincide. Starting from the diagram for mesh M1, next for M2, M3 and finally M4, it is observed that the load peaks get smaller and tend to the load-carrying capacity obtained in the experiment. An analogical order of the results is seen after the peak for softening. The solutions are closer and closer to the experimental response. Moreover, together with the mesh density growth, the differences between the diagrams decline. It is known that the LGD model requires a well-refined discretization (Wosatko, 2022) or a smart mesh densification near the expected cracking region (Negi *et al.*, 2021). Indeed, three meshes are sufficient to show the mesh-independent results for the CGD model. In the case of LGD model, the fourth mesh M4 has to be employed to prove that the consecutive solutions converge. Figures 5 and 6a depict the final distributions of  $\omega$  for case LGD-p-25. The crack patterns represented by damage have a similar character. Now the damage zone is clearly narrowed, so artificial widening of the damage distribution is eliminated, and the solution remains mesh-objective. Figure 6 contains enlarged plots for M4 to provide a better visibility against the background of this very dense mesh. Figure 6b shows the distribution of the gradient activity function  $\varphi_p$  in a reversed scale, i.e. the black colour indicates the smallest values. The shape of this distribution is slightly wider, but generally coincides with the damage distribution presented on the left in Fig. 6a.

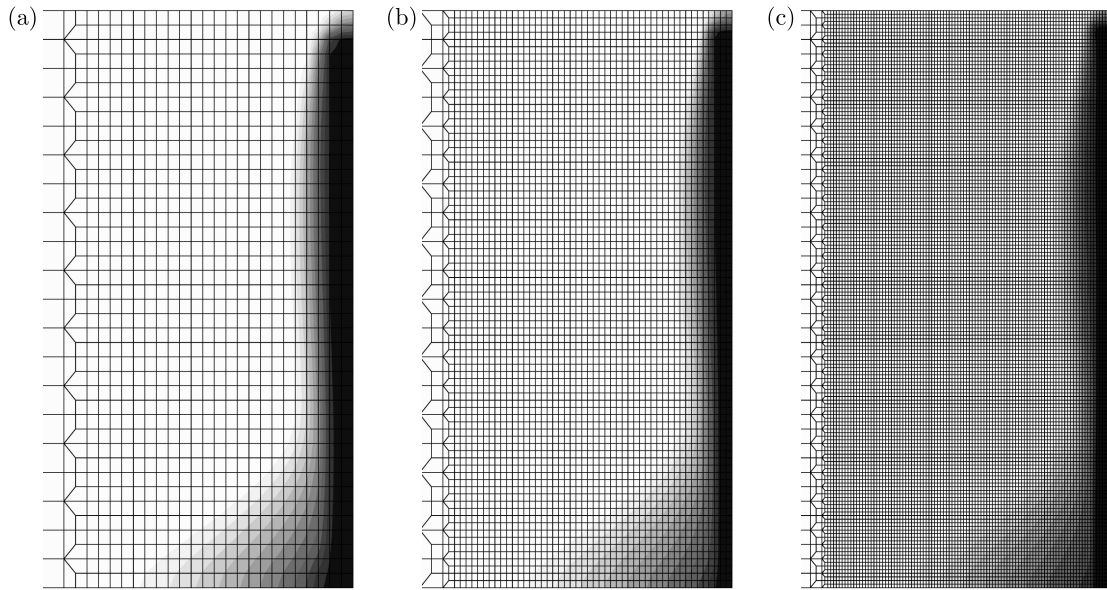


Fig. 5. Contour plots of damage  $\omega$  for LGD-p-25, mesh-sensitivity study: (a) mesh M1, (b) mesh M2, (c) mesh M3

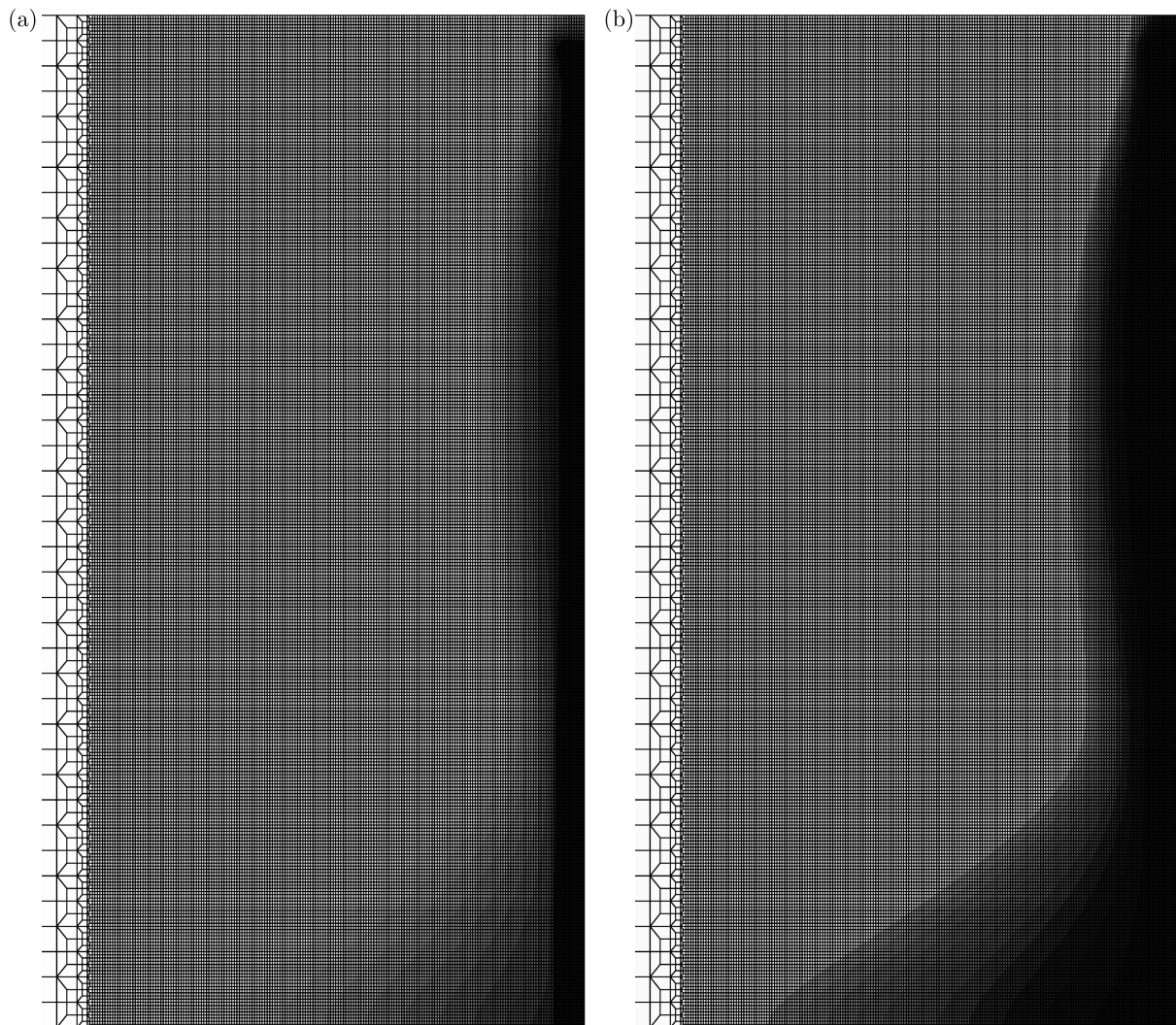


Fig. 6. Results for LGD-p25 and mesh M4: (a) damage  $\omega$ , (b) gradient activity  $\varphi_p(\omega)$  (reversed scale)

### 3.3. Size effect study

The results of the size effect study are discussed in this part of Section 3. Mesh M3 is selected for the computations for different specimen sizes, see Table 1. It should be reminded here that all experimental results are taken from Grégoire *et al.* (2013). Figure 7 juxtaposes the diagrams of the force  $F$  against the pseudo-CMOD  $u_{hor}$  for each beam, so that the confrontation between the experiment and responses for the cases defined in Table 2 can be carried out. The diagrams in Fig. 7a for the largest beam D1 are similar and differ only near the peak, however the curve after the peak for CGD gives a more brittle response. These equilibrium paths are over the limit of the gray zone coming from the experiment. The above observation changes together with reducing specimen dimensions. In Fig. 7b for beam D2, the response for the CGD model is more ductile than the others. The results for the LGD model are on the border of the gray region from the experiment. It is shown in Figs 7c and 7d for specimens D3 and D4 that CGD produces an exaggerated response, while the curves for options of the LGD model mostly fit the experimental results. They are different only for the maximum value of  $F$ , but in the same order for each beam size. Moreover, the cases LGD-c and LGD-p-01 overlap. The value of  $F$  for the case LGD-p-25 is below the previous two. The smallest  $F$  is obtained for the case LGD-e.

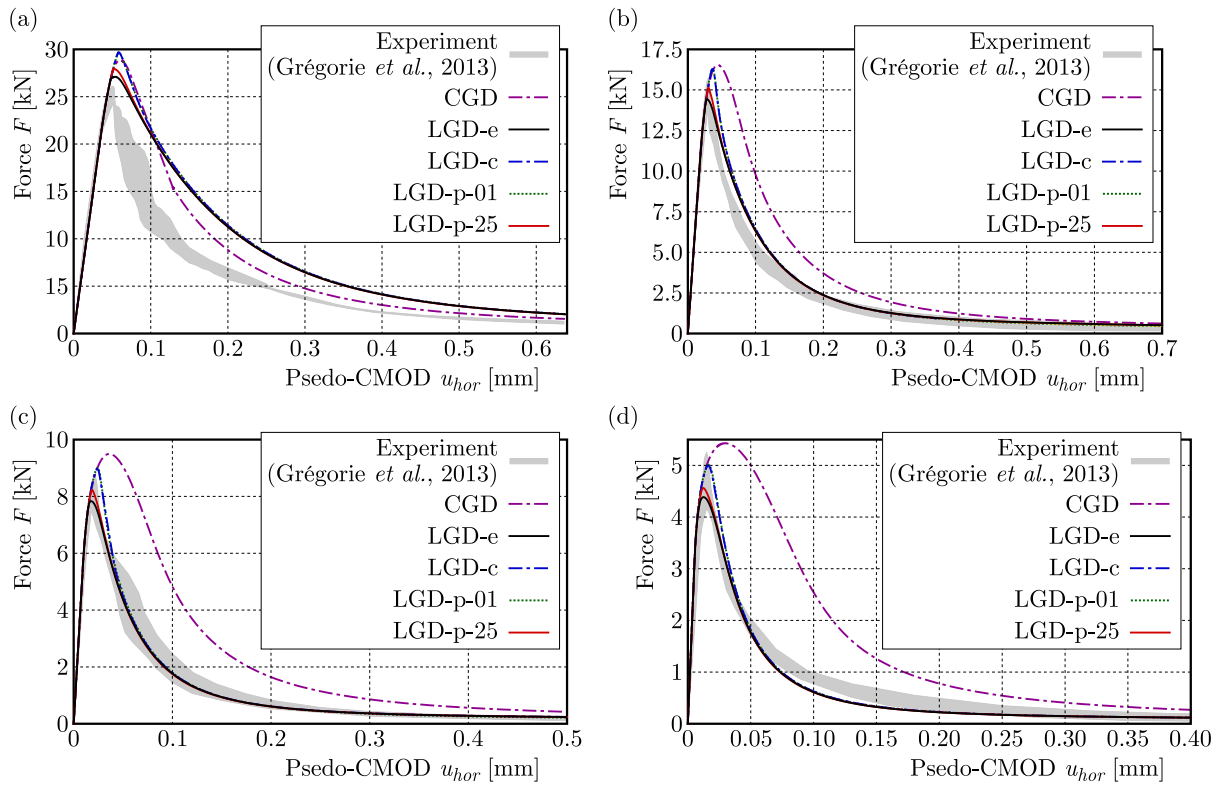


Fig. 7. Load vs. pseudo-CMOD diagrams – comparison between the employed models and experiment: (a) specimen D1, (b) specimen D2, (c) specimen D3, (d) specimen D4

Figures 8-11 present the FE meshes with final damage distributions for all cases given in Table 2 and, respectively, for all analyzed beams from Table 1. The undamaged areas, where  $\omega \approx 0.0$ , are represented by white colour, the gray scale shows the progress of cracking, and the total damage  $\omega \rightarrow 1.0$  is depicted by the black colour. It is illustrated for specimen D1 in Fig. 8 that the active damage is limited to a quite narrow band along the symmetry axis of the beam for each computed case, but the zone for CGD is slightly wider. It seems that the effect of excessive broadening for the CGD model intensifies for smaller sizes of the beam. It should

be noted that the crack zone widths should be similar, while the sizes of FEs change and are proportional to the growing beam dimensions. In other words, the beam size should have minor influence on the size of the FPZ. In fact, the issue of spuriously widened damage zone for the CGD model is visible, see Figs. 10a and 11a. This drawback does not reveal for the LGD model. Of course, the visualized crack band widths in the contour plots increase from specimen D1 (largest) to D4 (smallest), but the damage zone widths for the LGD model are relatively quite small and the increase of the widths does not seem proportional to the size reduction. It can be observed that the damage patterns for LGD-c and LGD-p-01 are almost identical, so it is confirmed that the function  $\varphi_c(\omega)$  with  $n = 1.0$  conforms with the function  $\varphi_p(\omega)$  with  $m = 0.1$ . On the other hand, similar damage distributions are obtained for cases LGD-e and LGD-p-25, i.e. the results for function  $\varphi_e(\omega)$  with  $n = 5.0$  and function  $\varphi_p(\omega)$  with  $m = 2.5$  are comparable.

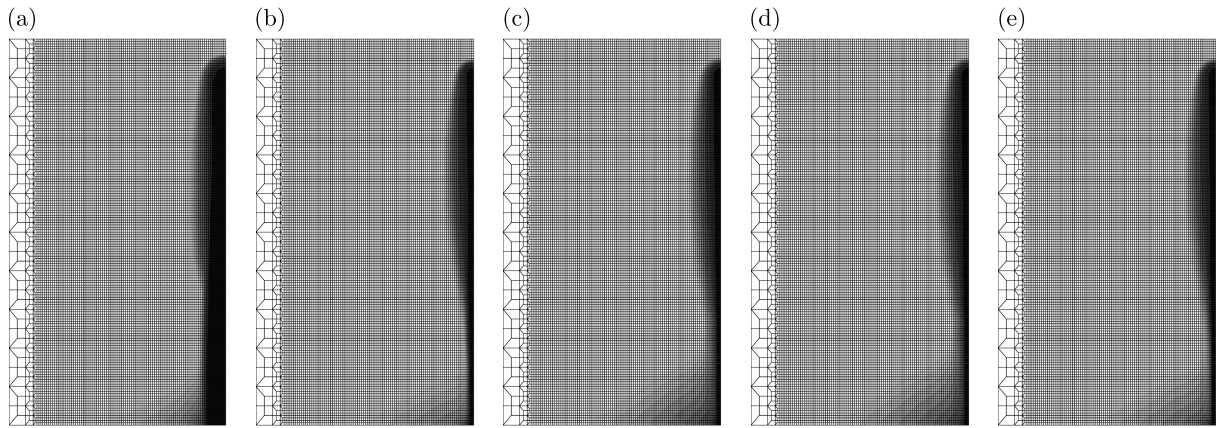


Fig. 8. Contour plots of damage  $\omega$  for specimen D1: (a) CGD, (b) LGD-e, (c) LGD-c, (d) LGD-p-01, (e) LGD-p-25

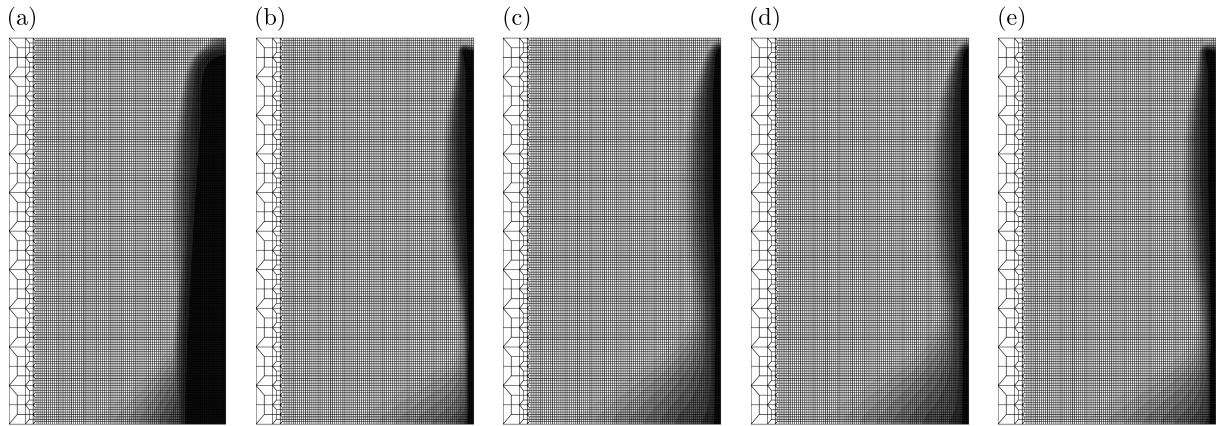


Fig. 9. Contour plots of damage  $\omega$  for specimen D2: (a) CGD, (b) LGD-e, (c) LGD-c, (d) LGD-p-01, (e) LGD-p-25

Figure 12 shows the diagrams of nominal stress  $\sigma_{nom}$  versus the horizontal strain  $\varepsilon$  for cases CGD and LGD-p-25. Both quantities are calculated in the following way. The nominal stress is

$$\sigma_{nom} = \frac{3}{2} \frac{FS}{TH^2} \quad (3.1)$$

and the horizontal strain is  $\varepsilon = u_{hor}/L_m$ . It is seen that the value of the nominal stress grows together with the decrease of the beam size. The response becomes also less brittle when the

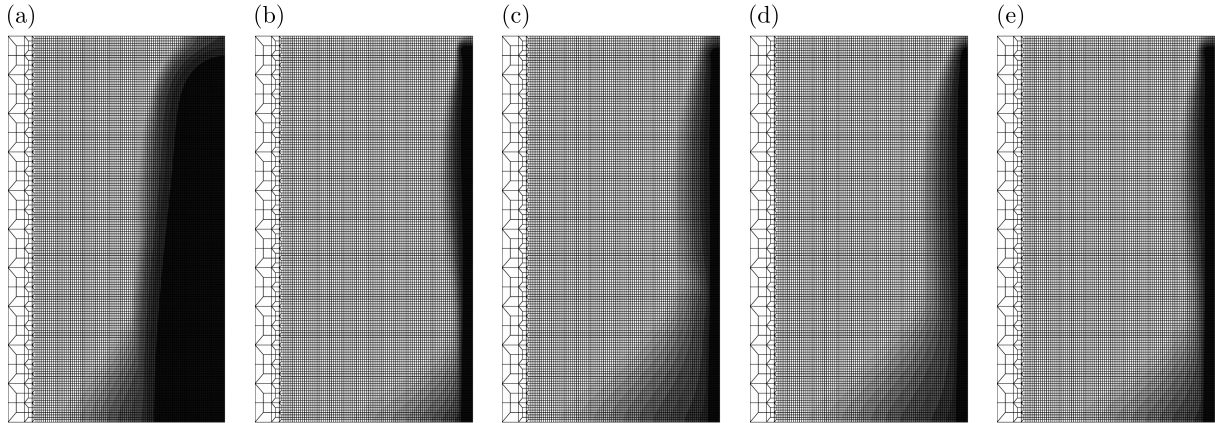


Fig. 10. Contour plots of damage  $\omega$  for specimen D3: (a) CGD, (b) LGD-e, (c) LGD-c, (d) LGD-p-01, (e) LGD-p-25

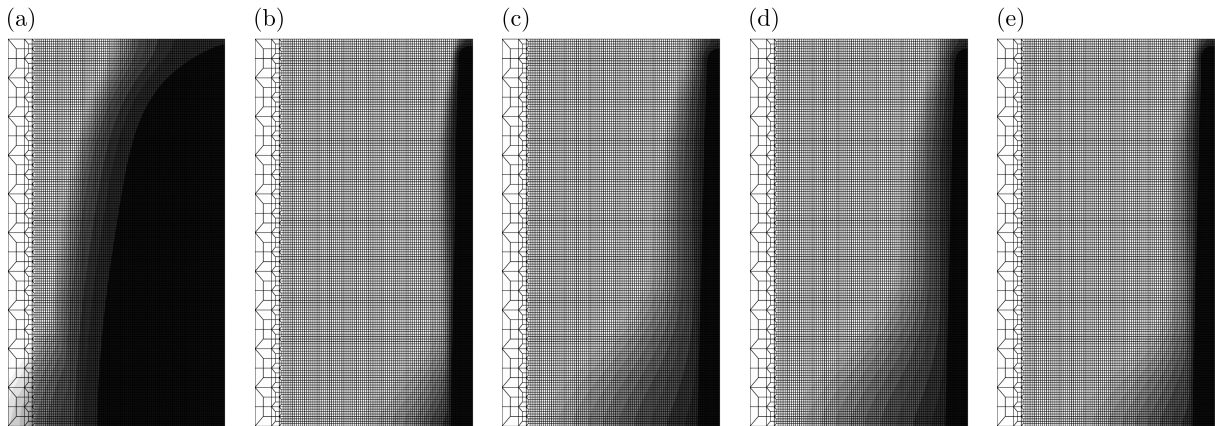


Fig. 11. Contour plots of damage  $\omega$  for specimen D4: (a) CGD, (b) LGD-e, (c) LGD-c, (d) LGD-p-01, (e) LGD-p-25

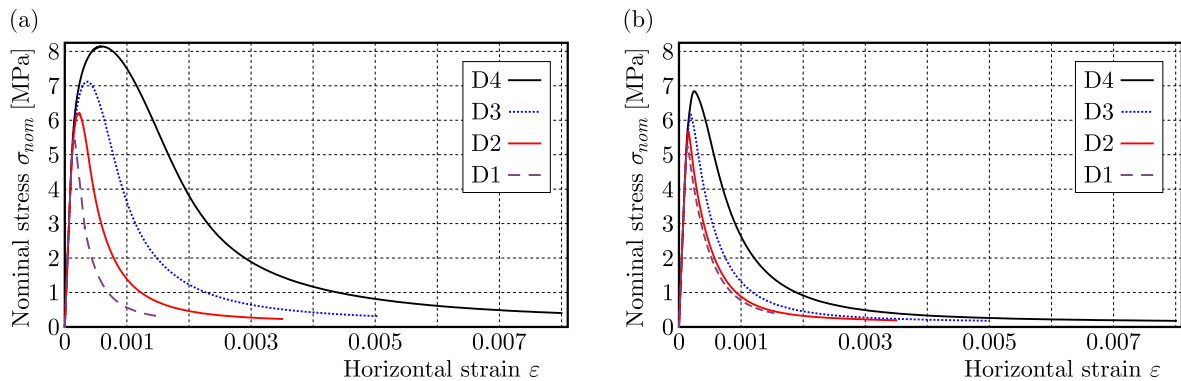


Fig. 12. Nominal stress vs horizontal strain diagrams – size effect study: (a) CGD, (b) LGD-p-25

specimen gets smaller. The CGD model demonstrates a much stronger size effect than the LGD-p-25. The size effect can also be verified based on Fig. 13, which is prepared in logarithmic scale for both axes. The nominal stress  $\sigma_{nom}$  is normalized by the tensile strength  $f_t$ , while the horizontal axis is determined by the proportion of beam heights  $H^i$  to the height  $H$  for specimen D4. The size effect is clearly visible for each case, but the results for CGD are over the zone representing the experiment.

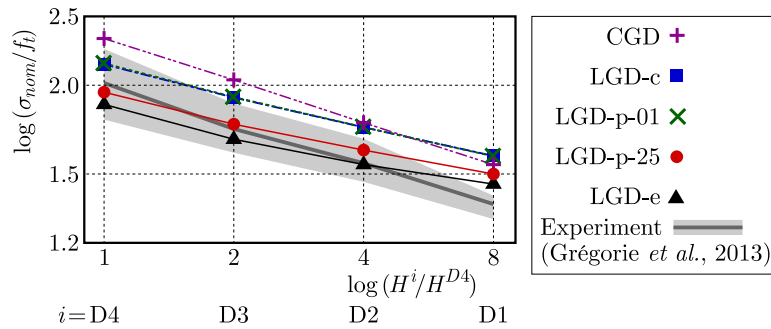


Fig. 13. Size effect plot – comparison between the employed models and experiment

#### 4. Conclusions

In general, non-local finite element models should be able to simulate the deterministic size effect, because a localization limiter introduces an internal length scale which sets the size of the FPZ, independent of the specimen size. Gradient damage models are equipped with such a internal length scale, which can be a constant parameter as for the conventional gradient damage (CGD) model, or a variable represented by a gradient activity function as for the localizing gradient damage (LGD) model.

In the paper, three definitions of the gradient activity function are described and compared in the simulations of the size effect. The function with exponential terms is known from Poh and Sun (2017). The function defined by cosine terms is suggested by Wosatko (2022). The function with polynomial terms, proposed by Borden (2012), de Borst and Verhoosel (2016), in the context of the phase-field model as a degradation function, is used for the first time in the LGD model. This function seems to have the most universal character.

The numerical analysis has been focused on a concrete beam under three point bending. The mesh sensitivity study has confirmed that the CGD model exhibits an issue of spuriously widened damage zone, and the LGD model is able to simulate a properly narrow localization band. The results of the numerical size effect study are compared with the experimental results provided by Grégoire *et al.* (2013). The obtained results are similar to those presented by Zhang *et al.* (2021) and Negi *et al.* (2021) but here, the analysis is focused on the employment of various gradient activity functions. Based on the results for the unnotched beam, it is demonstrated that the LGD model properly simulates the size effect and, for carefully adopted model parameters, the differences in the results for different gradient activity functions are small.

#### References

1. BARBAT G.B., CERVERA M., CHIUMENTI M., ESPINOZA E., 2020, Structural size effect: Experimental, theoretical and accurate computational assessment, *Engineering Structures*, **213**, 110555
2. BAŽANT Z.P., JIRÁSEK M., 2002, Nonlocal integral formulations of plasticity and damage: Survey of progress, *Journal of Engineering Mechanics – ASCE*, **128**, 11, 1119-1149
3. BAŽANT Z.P., LE J.-L., 2017, *Probabilistic Mechanics of Quasibrittle Structures. Strength, Lifetime, and Size Effects*, Cambridge University Press, Cambridge.
4. BAŽANT Z.P., OH B., 1983, Crack band theory for fracture of concrete, *RILEM Materials and Structures*, **16**, 155-177
5. BAŽANT Z.P., PLANAS J., 1998, *Fracture and Size Effect in Concrete and Other Quasibrittle Materials*, CRC Press, New York
6. BORDEN M.J., 2012, Isogeometric analysis of phase-field models for dynamic brittle and ductile fracture, Ph.D. Thesis, The University of Texas at Austin, Austin, Texas

7. CARMELIET J., 1999, Optimal estimation of gradient damage parameters from localization phenomena in quasi-brittle materials, *Mechanics of Cohesive-Frictional Materials*, **4**, 1, 1–16
8. DE BORST R., VERHOOSSEL C.V., 2016, Gradient damage vs. phase-field approaches for fracture: Similarities and differences, *Computer Methods in Applied Mechanics and Engineering*, **312**, 78-94
9. DE VREE J.H.P., BREKELMANS W.A.M., VAN GILS M.A.J., 1995, Comparison of nonlocal approaches in continuum damage mechanics, *Computers and Structures*, **55**, 4, 581-588
10. FENG D.-C., WU J.-Y., 2018, Phase-field regularized cohesive zone model (CZM) and size effect of concrete, *Engineering Fracture Mechanics*, **197**, 66-70
11. GARCÍA-ÁLVAREZ V.O., GETTU R., CAROL I., 2012, Analysis of mixed-mode fracture in concrete using interface elements and a cohesive crack model, *Sadhana*, **37**, 1, 187-205
12. GEERS M.G.D., 1997, Experimental analysis and computational modelling of damage and fracture, Ph.D. Thesis, Eindhoven University of Technology, Eindhoven
13. GRÉGOIRE D., ROJAS-SOLANO L.B., PIJAUDIER-CABOT G., 2013, Failure and size effect for notched and unnotched concrete beams, *International Journal for Numerical and Analytical Methods in Geomechanics*, **37**, 10, 1434-1452
14. HOOVER C.G., BAŽANT Z.P., VOREL J., WENDNER R., HUBLER M.H., 2013, Comprehensive concrete fracture tests: Description and results, *Engineering Fracture Mechanics*, **114**, 92-103
15. HORDIJK D.A., 1991, Local approach to fatigue of concrete, Ph.D. Thesis, Delft University of Technology, Delft
16. MAZARS J., PIJAUDIER-CABOT G., 1989, Continuum damage theory – application to concrete, *Journal of Engineering Mechanics – ASCE*, **115**, 2, 345-365
17. NEGI A., SINGH U., KUMAR S., 2021, Structural size effect in concrete using a micromorphic stress-based localizing gradient damage model, *Engineering Fracture Mechanics*, **243**, 107511
18. PEERLINGS R.H.J., DE BORST R., BREKELMANS W.A.M., DE VREE J.H.P., 1996, Gradient enhanced damage for quasi-brittle materials, *International Journal for Numerical Methods in Engineering*, **39**, 19, 3391-3403
19. PEERLINGS R.H.J., MASSART T.J., GEERS M.G.D., 2004, A thermodynamically motivated implicit gradient damage framework and its application to brick masonry cracking, *Computer Methods in Applied Mechanics and Engineering*, **193**, 30, 3403-3417
20. POH L.H., SUN G., 2017, Localizing gradient damage model with decreasing interaction, *International Journal for Numerical Methods in Engineering*, **110**, 6, 503-522
21. SAROUKHANI S., VAFADARI R., SIMONE A., 2013, A simplified implementation of a gradient-enhanced damage model with transient length scale effects, *Computational Mechanics*, **51**, 6, 899-909
22. TAYLOR R., 2001, *FEAP – A Finite Element Analysis Program, Version 7.4, User Manual*, University of California at Berkeley, Berkeley
23. WANG J., POH L.H., GUO X., 2022, Mixed mode fracture of geometrically similar FRUHPC notched beams with the localizing gradient damage model, *Engineering Fracture Mechanics*, **275**, 108843
24. WOSATKO A., 2022, Survey of localizing gradient damage in static and dynamic tension of concrete, *Materials*, **15**, 5, 1875
25. ZHANG Y., SHEDBALE A.S., GAN Y., MOON J., POH L.H., 2021, Size effect analysis of quasi-brittle fracture with localizing gradient damage model, *International Journal of Damage Mechanics*, **30**, 7, 1012-1035
26. ZHAO D., YIN B., TARACHANDANI S., KALISKE M., 2023, A modified cap plasticity description coupled with a localizing gradient-enhanced approach for concrete failure modeling, *Computational Mechanics*, **72**, 787-801